

# Ultrafast nanowire superconducting single-photon detector with photon number resolving capability.

Gregory N. Goltsman

Moscow State Pedagogical University, 1 Malaya Pirogovskaya, 119992, Moscow, Russia

## ABSTRACT

In this paper we present a review of the state-of-the-art superconducting single-photon detector (SSPD), its characterization and applications. We also present here the next step in the development of SSPD, i.e. photon-number resolving SSPD which simultaneously features GHz counting rate. We have demonstrated resolution up to 4 photons with quantum efficiency of 2.5% and 300 ps response pulse duration providing very short dead time.

**Keywords:** Superconducting single-photon detectors, photon number resolving detectors, ultrathin NbN films.

## 1. INTRODUCTION

Nanowire superconducting single-photon detector (SSPD) is a rapidly developing novel type of the detector. In terms of quantum efficiency, dark counts rate, maximum counting rate and timing resolution SSPD exhibits performances better than its semiconductor counterparts such as Si and InGaAs avalanche photodiodes (APDs). The best Si APDs<sup>1</sup> have 40 ps timing resolution,  $\approx 10 \text{ s}^{-1}$  dark counts rate, and maximum count rate about 3 MHz, their operational wavelength range is restricted by the energy gap in Si and thus their quantum efficiency drops rapidly at wavelength longer than  $1.1 \mu\text{m}$  making them unavailable for applications at telecom wavelengths. InGaAs APDs<sup>2</sup> have a wider wavelength band, up to  $1.8 \mu\text{m}$ , but they have worse timing resolution ( $\approx 300 \text{ ps}$ ) and suffer from very high dark counts rate ( $10^4 \text{ s}^{-1}$ ). Besides, both types of APDs need electrical quenching for fast operation.

SSPD outperforms its superconducting counterparts: although transition edge sensors (TES) were reported to have almost unity quantum efficiency at  $1.55 \mu\text{m}$  they are very slow (20 kHz maximum counting rate), have submicrosecond timing resolution and require operational temperature  $\approx 0.1 \text{ K}$ . Being capable to count infrared photons and having no intrinsic dark counts,<sup>3</sup> they are susceptible to triggering by mid-infrared photons.

Because of the favourable characteristics and the possibility to be effectively coupled to single-mode optical fiber<sup>4,5</sup> together with an installation into closed cycle refrigerator system<sup>6</sup> many applications of the SSPD have already been reported. The most impressive one is the report on the quantum key distribution (QKD) over 200 km distance.<sup>7</sup> Other QKD experiments also were reported<sup>8</sup> as well as non-quantum optical communication.<sup>9</sup> The implementation of the SSPD for the research into emission of single-photon sources, e.g. quantum dots or quantum wells, by time-correlated single-photon counting methods were reported in.<sup>5,10-13</sup> Recently several experiments on quantum information processing with SSPD have been reported as well.<sup>14,15</sup>

In this paper we give a review of the state-of-the-art SSPD technology: fabrication, operation principles, performances, photon number resolving capability, and optical applications of SSPD.

## 2. THE STATE-OF-THE-ART SSPD: OPERATION PRINCIPLES, FABRICATION, PERFORMANCE AND APPLICATIONS

### 2.1 Operation principles, design and fabrication

SSPD is essentially a nanodevice made of 4-nm-thick NbN film. Its sensitive element is 120-nm-wide superconducting strip patterned as a meander covering  $10 \mu\text{m} \times 10 \mu\text{m}$  area<sup>16</sup> embedded in a  $50 \Omega$  co-planar line. Fig. 1 presents the design of the on-chip SSPD co-planar line and SEM image of the SSPD sensitive element.

---

Further author information: (Send correspondence to Gregory Goltsman)  
E-mail: goltsman@mospu-phys.ru, Telephone: +7 499 246 12 02

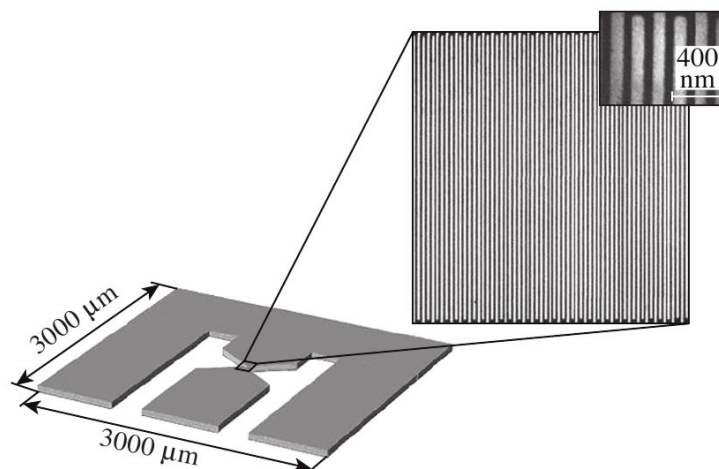


Figure 1. SEM image of the  $10\ \mu\text{m} \times 10\ \mu\text{m}$  NbN meander comprising the SSPD and  $3\ \text{mm} \times 3\ \text{mm}$  gold contacts mating  $50\ \Omega$  co-planar line.

Operation principle of the SSPD is based on the formation of a resistive region across the thin and narrow superconducting film maintained at a temperature well below its critical temperature  $T_c$  and carrying bias current  $I_b$  close to the critical current  $I_c$  of the strip.<sup>17,18</sup>

The SSPD fabrication process was described in detail in<sup>19</sup> and here we give a brief description. NbN superconducting films are deposited on R-cut or M-cut sapphire substrates by a dc reactive magnetron sputtering in an Ar and  $\text{N}_2$  mixture. The film characteristics are as follows: surface resistance  $R_S=380\text{--}500\ \Omega/\text{sq}$ , critical temperature  $T_c=10\text{--}11\ \text{K}$ , superconducting transition width  $\Delta T_c \approx 0.3\ \text{K}$ , and critical current density  $j_c = 3 - 5 \times 10^6\ \text{A}/\text{cm}^2$  at 4.2 K. Details of our thin NbN film fabrication process are described in.<sup>20</sup> The patterning of the meander is performed by means of electron beam lithography and reactive ion etching. Large-scale elements such as contact pads and alignment marks are patterned by photolithography and wet etching.

## 2.2 Performance

In visible and near infrared (up to  $1.3\ \mu\text{m}$  wavelength) SSPD has quantum efficiency  $QE$  (the ratio of the detection events to the number of photons falling on the SSPD) up to 30% which is its ultimate value limited by the NbN film absorption. Typically SSPD exhibits such a performance at about 2 K operation temperature. Fig. 2 presents SSPD  $QE$  vs bias current for 4.2 K and 2.2 K temperatures for  $1.3\ \mu\text{m}$  wavelength. One can see that  $QE$  at 4.2 K is about 4 times smaller. Recently we reported about an SSPD that exhibit  $QE = 30\%$  at 4.2 K temperature<sup>16</sup> (Fig. 3). Although such SSPDs are quite rare so far, it is mostly a matter of the fabrication process optimization. Such devices are very attractive for application in cryocoolers since 4 K cryocoolers are cheaper, more compact and have less power consumption compared to 2 K models. There are also reports about successful integration of SSPDs with microcavities<sup>21,22</sup> which allows one to increase  $QE$  up to 60%.<sup>22</sup>

SSPD has a broadband spectral sensitivity up to  $5\text{--}6\ \mu\text{m}$  wavelengths. Solid curve in Fig. 4 presents SSPD  $QE$  vs wavelength measured at 5 K temperature with black body source and a grating spectrometer, whereas single points (black squares) present SSPD  $QE$  measured at 1.7–2 K temperature with light emitting diodes. One can see that with the increase of the wavelength one can observe a decrease of  $QE$ , i.e. at 2 K temperature at  $1.5\ \mu\text{m}$   $QE = 17\%$  while in middle infrared SSPD exhibits  $QE = 0.4\%$  at 1.7 K temperature<sup>16,23</sup> making SSPD almost the only practical fast single-photon detector in this wavelength range.

SSPD combines high  $QE$  with negligibly low level of dark count rate  $R_{dk}$ . It was reported that minimum  $R_{dk}$  value is as low as  $2 \times 10^{-4}\ \text{s}^{-1}$  which was measured at 2 K temperature when SSPD input was completely blocked.<sup>24</sup> Together with high  $QE$  it allows one to achieve noise equivalent power as low as  $5 \times 10^{-21}\ \text{W}/\text{Hz}^{1/2}$  at

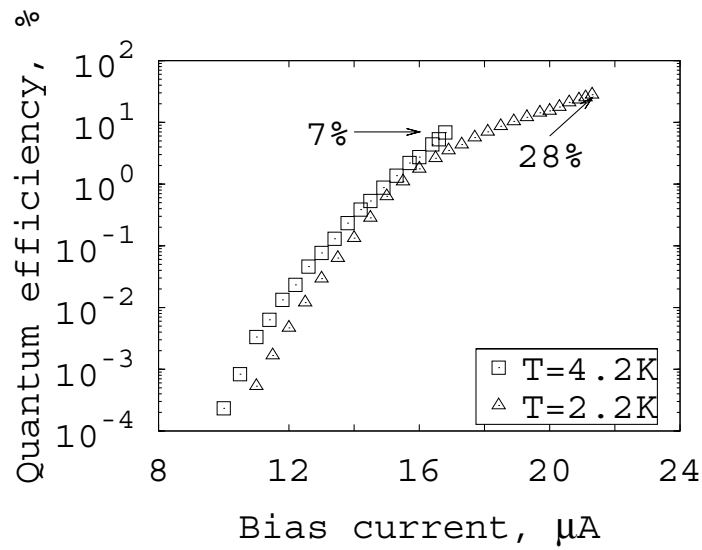


Figure 2. Quantum efficiency vs bias current at 2.2 K and 4.2 K temperatures for a typical SSPD.

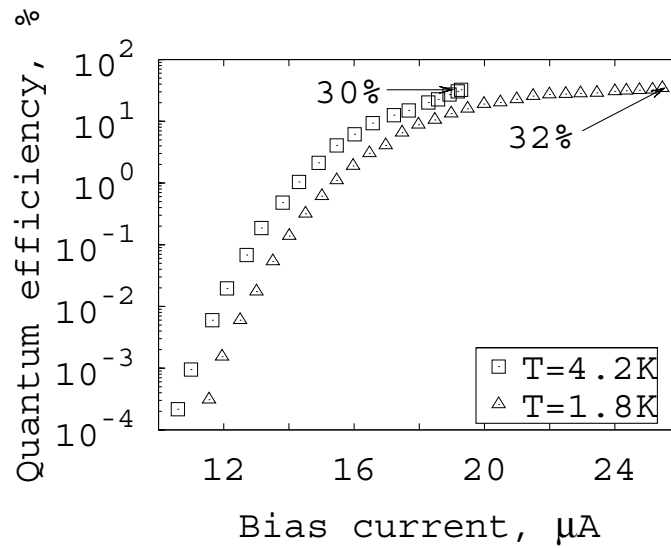


Figure 3. Quantum efficiency vs bias current at 1.8 K and 4.2 K temperatures for one of the best SSPDs.

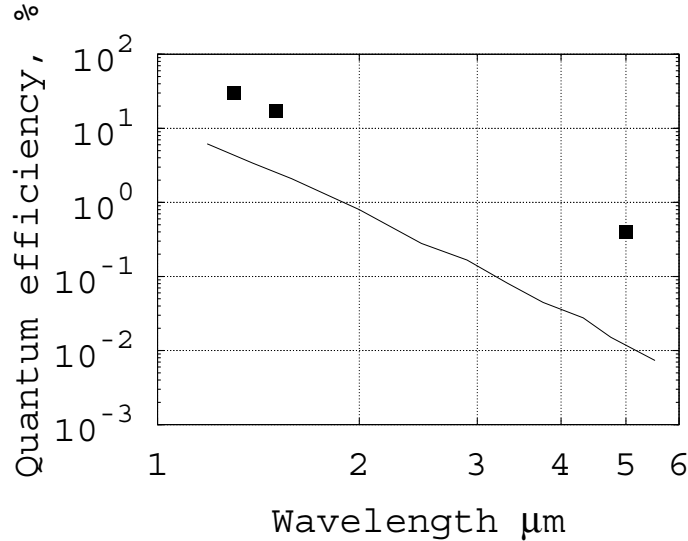


Figure 4. SSPD quantum efficiency vs wavelength measured with a grating spectrometer (solid line) at 5 K temperature and infrared light emitting diodes (black squares) at 1.6 K temperature. At 5  $\mu\text{m}$  wavelength SSPD exhibits  $QE=0.4\%$ .

1.3  $\mu\text{m}$  and  $1 \times 10^{-18}$   $\text{W}/\text{Hz}^{1/2}$  at 5  $\mu\text{m}$  wavelengths.<sup>16</sup> Although such low values are unreachable in a practical situation they can be considered as ultimate values for this type of a single-photon detector.

Timing characteristics (jitter and counting rate) make SSPD competitive with other single-photon detectors. SSPD timing jitter is as low as 18 ps including jitter of read-out electronics.<sup>25</sup> It was derived from a histogram of delay between the SSPD response and the laser trigger by the standard feature of the oscilloscope. In<sup>12</sup> a 74 ps timing jitter was reported for a fiber-coupled SSPD measured by a photon correlation technique. This value includes all electronic jitter which is evaluated to be under 30 ps. Due to kinetic inductance limitation of the SSPD reset time<sup>26</sup> the maximum counting rate was limited by about 100 MHz. Recently we found a solution to this problem (see below) which allowed us to reduce the reset time to subnanosecond range and provide GHz counting rate.

### 3. PRACTICAL TWO-CHANNEL SINGLE-PHOTON RECEIVER SYSTEM

We developed a two-channel single-photon receiver system based on fiber-coupled SSPDs and designed for applications in quantum communication and quantum optics research such as antibunching-type correlation studies of near-infrared photons emitted by semiconductor quantum dots. In<sup>4,27</sup> a successful realization of a similar system with fiber coupled SSPDs was reported. A ring made from photoresist was used to ensure alignment of the fiber against the NbN meander of SSPD and the SSPDs were operated in a standard storage dewar at 4.2 K temperature. In<sup>12</sup> we reported a system having two major differences was reported: a method of SSPD coupling and its operation temperature, both leading to a significant improvement of the system performance. A mechanical alignment of the SSPD against the fiber was used instead of photoresist ring, and we improved the system to enable SSPD operation at 2 K temperature being immersed in a transport dewar.

The system is designed as a double-wall insert with vacuum insulation (Fig. 5). Liquid helium from the storage dewar penetrates into the inner volume of the insert through the filter and the capillary. To achieve a temperature below 4.2 K the liquid helium vapor is pumped from the inner volume. The capillary limits the speed of liquid helium penetration and allows a vapor pressure of 80–120 Pa and a temperature of 1.6 K to be obtained.

The system has two identical photon detecting channels. Two SSPDs (one in each channel) are coupled to the single-mode optical fibers and mounted at the bottom of the inner volume of the insert in the liquid helium. The SSPDs are aligned against the fibers with the standalone micromechanical positioner and then glued to the device holder. When SSPDs are fixed in this way the positioner is removed. Electrical contact is realized

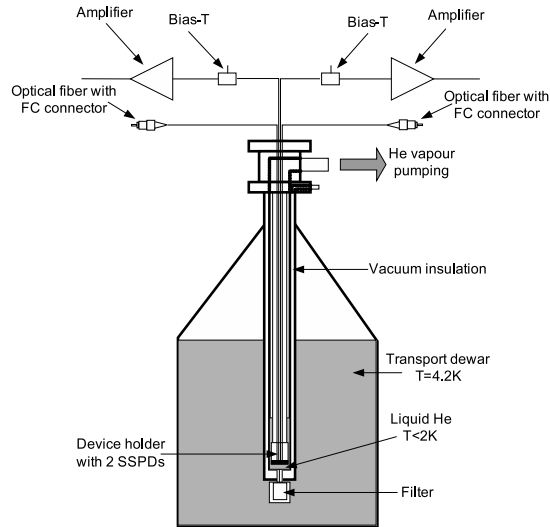


Figure 5. Two-channel single-photon receiver system design

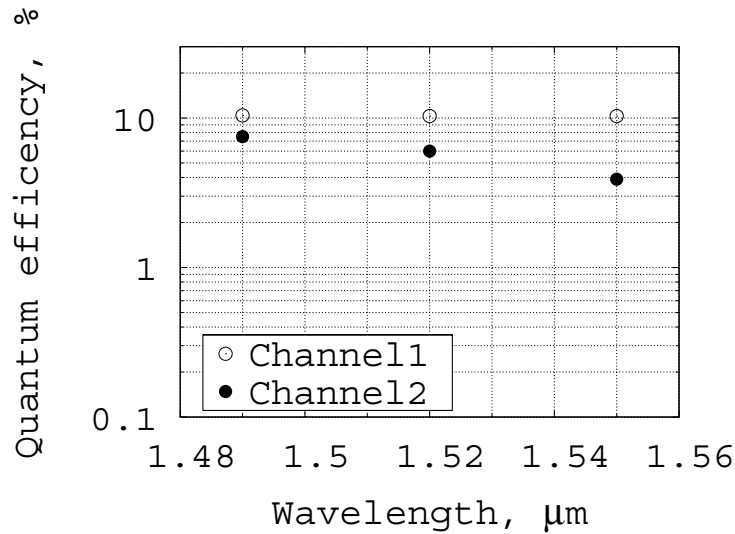


Figure 6. Quantum efficiency vs wavelength measured for both channels of the single-photon receiver at 1 Hz of dark counts rate.

through co-planar waveguides and coaxial cables connected to two room temperature bias-Ts. For DC bias we use a home-built current/voltage source. The SSPD photoresponse voltage pulse is transmitted by the coaxial cable to the room-temperature amplifiers, one in each channel (60 dB gain) producing pulses larger than 0.5 V. Then the signals from the channels are fed to the discriminators and to the counter and oscilloscope or to the coincidence circuit depending on the goals of experiment.

The temperature is controlled by the efficiency of pumping and is measured with the thermometer mounted on the same holder as the SSPDs. The minimum achievable temperature is mostly determined by the capabilities of the pump and can be as low as 1.6 K. Temperature below 2 K can be achieved with a pump performance above 5 m<sup>3</sup>/hour.

A filtering of thermal room temperature background radiation allowed us to reduce the dark counts rate  $R_{dk}$  by several orders of magnitude.<sup>5</sup>

Improved method of SSPD coupling with the reduction of  $R_{dk}$  allowed us to achieve the maximum system quantum efficiency ( $QE$  reduced to the input of the fiber) above 10% at 1.55 μm wavelength (Figure 6) at dark count rate of 1–2 counts per second.

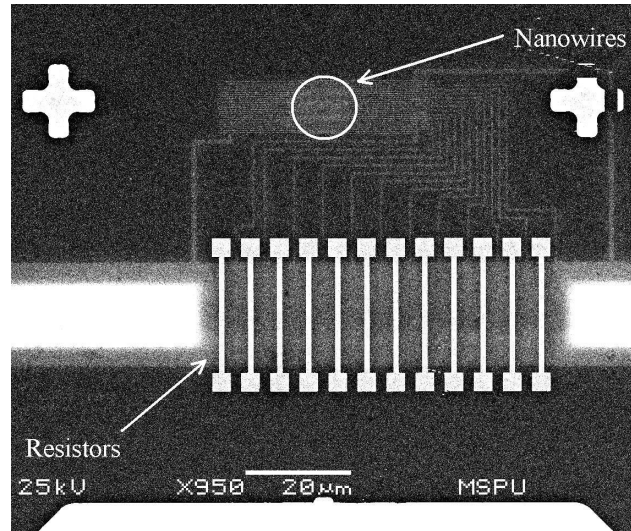


Figure 7. SEM image of the 12-section “parallel wire” SSPD. Each section is a meander-shaped nanowire patterned in the same way as usual SSPD, the width of the wire is 120 nm, the gap between the wires is 80 nm. The resistors are made from 30-nm-thick gold film and serve for uniform current distribution among the wires and allows for operation closer to the critical current.

#### 4. FAST SSPD DESIGN AND FABRICATION

As it was demonstrated by A. Kerman *et al*<sup>26</sup> the response time of the SSPD is limited by the kinetic inductance of the SSPD. To reduce the kinetic inductance we divided one long meander-shaped nanowire in several parts of equal length and connected them in parallel. Each part is a meander-shaped nanowire and all parts are placed close to each other and cover the same square area of  $10\ \mu\text{m} \times 10\ \mu\text{m}$ . Indeed, by division a nanowire with the kinetic inductance  $L_0$  in  $N$  equal parts we reduce the kinetic inductance of each wire by the factor of  $N$ . If we connect those  $N$  wires in parallel their equivalent inductance is reduced by the factor of  $N^2$  compared to  $L_0$ . It leads to  $N^2$  shorter reset time of the “parallel wire” SSPD compared to usual single-wire SSPD.

The “parallel wire” SSPD fabrication process is based on the well developed process of the usual SSPD fabrication described in detail in.<sup>19</sup> It is based on e-beam lithography and reactive ion etching. Figure 7 presents a 12-section “parallel wire” SSPD. Each section is a meander-shaped nanowire patterned in the same way as usual SSPD. The width of the wire is 120 nm, the gap between the wires is 80 nm. The total area covered by the nanowires is  $10\ \mu\text{m} \times 10\ \mu\text{m}$ . To ensure uniform bias current distribution between the nanowires each nanowire is connected to a planar resistor made of 30-nm-thick gold film. The resistance is in range 1–100 Ohm and depends on the number of parallel nanowires. These resistors serve one more function, i.e. they allow for operation of “parallel wire” SSPD at a bias current close to its critical current. The “parallel wire” SSPD is operated in a constant-current regime. If a nanowire becomes resistive its current drops whereas bias currents of other nanowires increase. The resistors suppress this unwanted increase of the bias current.

For precise “parallel wire” SSPD response time characterization we used a setup with 12-GHz-band amplifiers and a sampling oscilloscope. The photoresponse characteristic time was derived directly from waveform transients and was taken as  $1/e$  fall or rise time. We studied SSPDs consisting of 2, 5 and 12 nanowires connected in parallel. For all of them the total area covered by the nanowires was  $10\ \mu\text{m} \times 10\ \mu\text{m}$ . Fig. 8 presents the waveform transients for SSPDs consisting of 12 and 5 parallel sections (upper plot). The insert shows 16-ps jitter of the 12-section “parallel wire” SSPD measured with the pulsed laser with a built-in feature of the oscilloscope. In Fig. 8 (bottom plot) we also plotted the characteristic fall times vs number of parallel nanowires.<sup>28</sup> We also plotted  $1/N^2$  law (solid line) which fall times should obey to. The fall time is taken as a time during which the voltage reduces by a factor of  $e$ . The insert of the bottom plot describes how the fall time is taken. From the  $1/N^2$  fitting curve in Figure 8 we can estimate the kinetic inductance of one-section SSPD to be equal to  $\approx 500$  nH which is in a reasonable agreement with the results reported in<sup>26</sup> for similar devices.

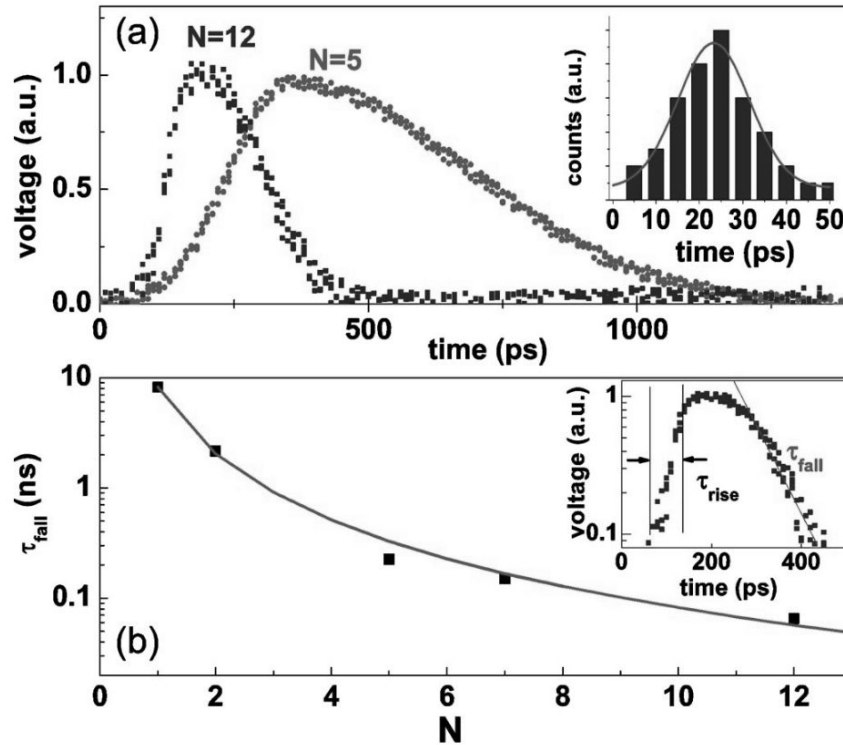


Figure 8. Waveform transients for SSPDs consisting of 12 and 5 parallel sections (upper plot), the insert shows 16-ps jitter of the 12-section “parallel wire” SSPD. The bottom plot shows the dependence of the fall time (taken as  $1/e$ , see the insert) on the number of parallel wires.

## 5. PHOTON NUMBER RESOLVING SSPD

Division of a nanowire in several parts connected in parallel enables the SSPD to distinguish the number of photons simultaneously falling on its surface. Indeed, when a photon is absorbed by a nanowire that nanowire becomes resistive. Although at first glance it seems that other sections should act like a shunt but this does not actually happen due to the kinetic inductance of those sections. As a result a voltage appears on the terminals of the SSPD. If two photons make two different sections resistive the response voltage is almost twice higher than from one photon. Three photons absorbed by three sections produce three times higher response. This mechanism allows one to distinguish the number of photons absorbed simultaneously by the magnitude of the response voltage.

The experimental setup (Fig. 9) consisted of a pulsed semiconductor laser (operating at  $0.85\text{-}\mu\text{m}$  wavelength with 30-ps pulse width and 100 kHz maximum repetition rate) which radiation was fed into a fiber and then divided in two equal parts. One part was fed to the powermeter whereas the other part was fed to the “photon number resolving” SSPD (PNR-SSPD) coupled to a fiber and maintained in a liquid helium at 4.2 K temperature. Electrical photoresponse pulse was fed to a coaxial cable and then to amplifiers (500 MHz band,  $\approx 70$  dB amplification) and a pulse counter and a single-shot oscilloscope. The laser and the oscilloscope were triggered from a single impact generator. To vary a power of the radiation falling on the PNR-SSPD we used a variable fiber-based optical attenuator.

Fig. 10 presents the photoresponse waveform transients taken from the single-shot oscilloscope. Although the waveforms are seriously affected by the amplifiers band (in reality the pulses are significantly shorter), four different amplitudes are easily observed. With the increase of the number of photons in the laser pulse incident on the SSPD, the probability to observe higher response amplitude increases.

To prove that the responses of different magnitude correspond to different number of photons we used the following treatment. Assuming an ideal detector with 100% quantum efficiency, for a mean number of  $m$  photons

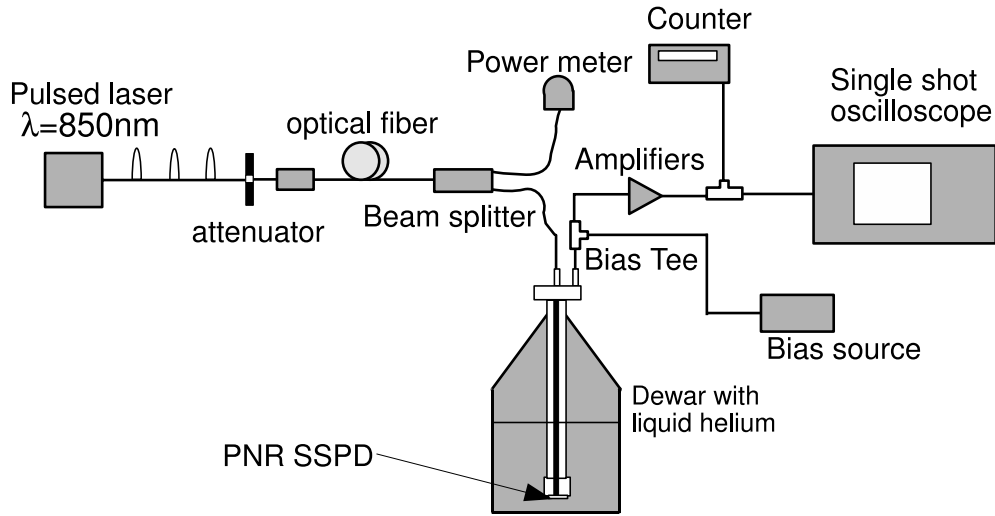


Figure 9. Experimental set-up for PNR-SSPD characterization.

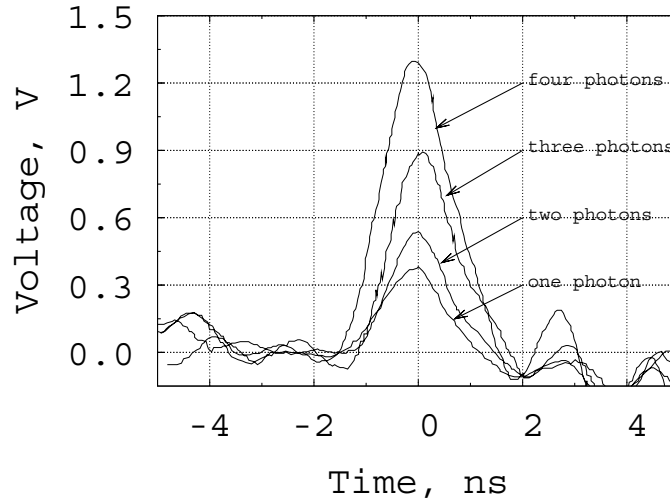


Figure 10. PNR-SSPD waveform transients resulting from simultaneous detection of 1–4 photons.

per pulse, the probability  $P(n)$  of detecting  $n$  photons from a given pulse is  $P(n) \propto (e^{-m}m^n)/(n!)$ . When  $m \ll 1$  the probability  $P(n)$  simplifies to

$$P(n) \propto \frac{m^n}{n!} \quad (1)$$

Consequently, the probability of detecting one photon is proportional to  $m$ , the probability of detecting two photons is proportional to  $m^2$ , and so on. In spite of the fact that the SSPD under test had its quantum efficiency well below 100% the above treatment is in force provided that we consider actually detected photons instead of photons in the laser pulse (in this case the number of photons falling on the SSPD may be much more than 1).

Fig. 11 presents relative detection probability vs optical attenuation of laser pulse for the pulses of three different magnitudes. Top curve (squares) corresponds to the pulses of smallest magnitude (“one photon” in Fig. 10). The middle curve (triangles) in Figure 11 is taken for the pulses of higher magnitude (“two photons” in Fig. 10). The third curve (circles) is taken for the “three photons” curve in Fig. 10. The results in Fig. 11 follows equation 1 and demonstrates clearly the capability of the detector to resolve one, two and three photons simultaneously detected.

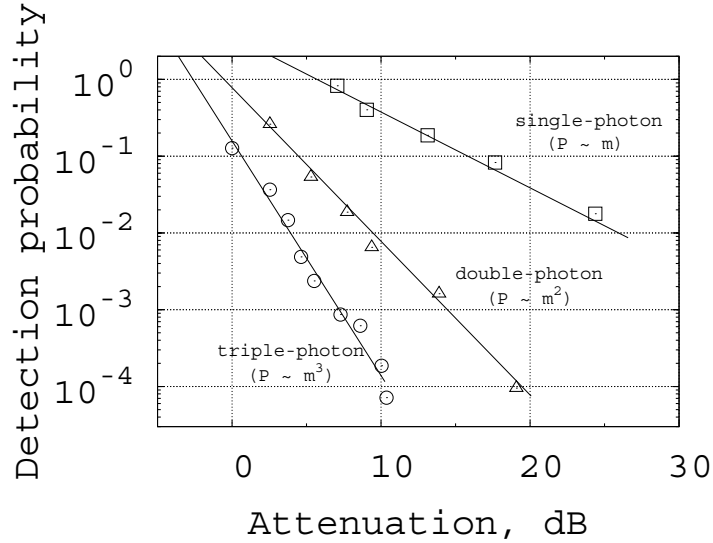


Figure 11. Detection probability vs incident power measured for three different magnitudes of photoresponse that clearly proves unambiguous correspondence of the photoresponse magnitude to the number of simultaneously detected photons.

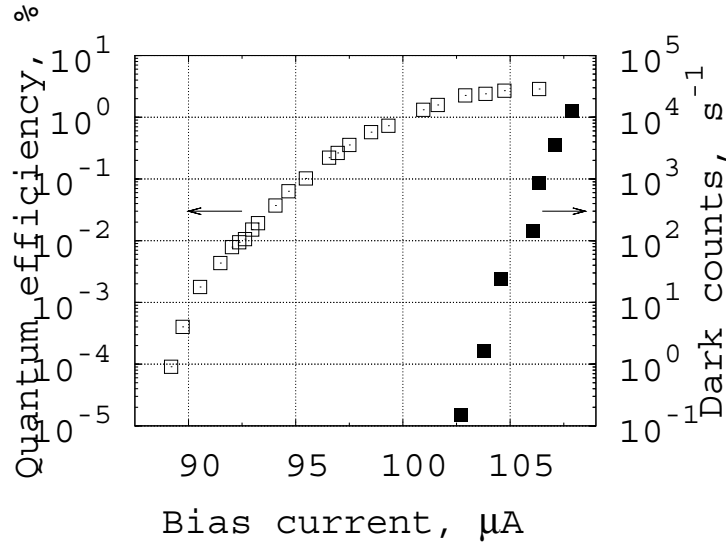


Figure 12. PNR-SSPD quantum efficiency and dark counts rate vs bias current measured at 2 K temperature.

Finally, we measured quantum efficiency  $QE$  at  $1.3 \mu\text{m}$  wavelength and dark counts rate  $R_{dk}$  of the PNR-SSPD. Figure 12 presents these results measured at 2.2 K temperature. One can see that the PNR-SSPD exhibits  $QE \approx 2.5\%$  and  $R_{dk} \approx 0.1 \text{ s}^{-1}$ .

## 6. CONCLUSION

We presented a review of the state-of-the-art SSPD which manifests up to 30% quantum efficiency at  $1.3 \mu\text{m}$ , 17% at  $1.5 \mu\text{m}$  and 0.4% at  $5 \mu\text{m}$  wavelengths with negligibly low dark counts rate and 16 ps timing jitter. Connection of nanowires in parallel allowed us to reduce the kinetic inductance and achieve 300 ps response time which enables GHz counting rate. We also presented a photon-number resolving SSPD which is presently capable to resolve up to 4 simultaneously absorbed photons. Improvement of quantum efficiency of such PNR-SSPD and its successful coupling to single-mode optical fiber will make possible its installation in the described above two-channel single-photon receiver. It will make PNR-SSPD available for many experimental and practical applications such as research into multi-photon sources and realization of multi-photon protocols in quantum cryptography.

## ACKNOWLEDGMENTS

The authors would like to thank Dr. T. Debuisschert and Dr. A. Beveratos for help in characterization of two-channel single-photon receiver system at 1.55  $\mu\text{m}$  wavelength and Dr. J. Ph. Poizat for “parallel wire” SSPD timing characterization.

This work was supported in part by EU FP6 STREP ”SINPHONIA” (contract number NMP4-CT-2005-16433), the grant ”Non-equilibrium processes after IR photon absorption in thin-film superconducting nanostructures” of Russian Agency on education, Russian Foundation for Basic Research grant 07-02-13626.

## REFERENCES

- [1] Cova, S., Ghioni, M., Lacaita, A., Samori, C., and Zappa, F., “Avalanche photodiodes and quenching circuits for single-photon detection,” *Applied Optics* **35**(12), 1956 (1996).
- [2] Zappa, F., Lacaita, A., Cova, S., and Webb, P., “Nanosecond single-photon timing with ingaas/inp photodiodes,” *Optic Letters* **19**(11), 846 (1994).
- [3] Rosenberg, D., Lita, A., Miller, A., and Nam, S. W., “Noise-free high-efficiency photon-number-resolving detectors,” *Phys. Rev. A* **71**, 061803(R) (2005).
- [4] Slys, W., Wegrzecki, M., Bar, J., Gorska, M., Zwiler, V., Latta, C., Bohi, P., Milostnaya, I., Minaeva, O., Antipov, A., Okunev, O., Korneev, A., Smirnov, K., Voronov, B., Kaurova, N., Gol’tsman, G., Pearlman, A., Cross, A., Komissarov, I., Verevkin, A., and Sobolewski, R., “Fiber-coupled single-photon detectors based on nbn superconducting nanostructures for practical quantum cryptography and photon-correlation studies,” *Applied Physics Letters* **88**, 261113 (2006).
- [5] Zinoni, C., Alloing, B., Li, L. H., Marsili, F., Fiore, A., Lunghi, L., Gerardino, A., Vakhtomin, Y. B., Smirnov, K. V., and Gol’tsman, G. N., “Single-photon experiments at telecommunication wavelengths using nanowire superconducting detectors,” *Appl. Phys. Lett.* **91**, 031106 (2007).
- [6] Hadfield, R., Stevens, M., Gruber, S., Miller, A., Schwall, R., Mirin, R., and Nam, S. W., “Single photon source characterization with a superconducting single photon detector,” *Optics Express* **13**(26), 10846 (2005).
- [7] Takesue, H., Nam, S. W., Zhang, Q., Hadfield, R., Honjo, T., Tamaki, K., and Yamamoto, Y., “Quantum key distribution over a 40-dB channel loss using superconducting single-photon detectors,” *Nature Photonics* **1**, 343–348 (2007).
- [8] Hadfield, R., Habif, J., Schlafer, J., Schwall, R., and Nam, S. W., “Quantum key distribution at 1550 nm with twin superconducting single-photon detectors,” *Applied Physics Letters* **89**, 241129 (2006).
- [9] Robinson, B., Kerman, A., Dauler, E., Barron, R., Caplan, D., Stevens, M., Carney, J., Hamilton, S., Yang, J., and Berggren, K., “781-Mbit/s photon-counting optical communications using a superconducting nanowire detector,” *Optics Letters* **31**, 444–446 (2006).
- [10] Stevens, M., Hadfield, R., Schwall, R., Nam, S. W., Mirin, R., and Gupta, J., “Fast lifetime measurements of infrared emitters using a low-jitter superconducting single-photon detector,” *Applied Physics Letters* **89**, 031109 (2006).
- [11] Stevens, M., Hadfeld, R., Schwall, R., Nam, S. W., and Mirin, R., “Quantum dot single photon sources studied with superconducting single photon detectors,” *IEEE Journal of Selected Topics in Quantum Electronics* **12**(6), 1255 (2006).
- [12] Korneev, A., Vachtomin, Y., Minaeva, O., Divochiy, A., Smirnov, K., Okunev, O., Goltsman, G., Zinoni, C., Chauvin, N., Balet, L., Marsili, F., Bitauld, D., Alloing, B., Lianhe, L., Fiore, A., L. Lunghi, A. G., Halder, M., Jorel, C., and Zbinden, H., “Single-photon detection system for quantum optics applications,” *IEEE Journal of Selected Topics in Quantum Electronics* **13**(4), 944–951 (2007).
- [13] Hostein, R., Michon, A., Beaudoin, G., Gogneau, N., Patriache, G., Marzin, J.-Y., Robert-Philip, I., Sagnes, I., and Beveratos, A., “Time-resolved characterization of InAsP/InP quantum dots emitting in the C-band telecommunication window,” *Appl. Phys. Lett* **93**, 073106 (2008).
- [14] Chen, J., Altepeter, J., Medic, M., Lee, K. F., Gokden, B., Hadfield, R., Nam, S. W., and Kumar, P., “Demonstration of a quantum controlled-NOT gate in the telecommunications band,” *Phys. Rev. Lett.* **100**, 133603 (2008).

- [15] Halder, M., Beveratos, A., Gisin, N., Scarani, V., and C. Simon, H. Z., “Entangling independent photons by time measurement,” *Nature Physics* **3**, 692 (2007).
- [16] Goltsman, G., Minaeva, O., Korneev, A., Tarkhov, M., Rubtsova, I., Divochiy, A., Milostnaya, I., Chulkova, G., Kaurova, N., Voronov, B., Pan, D., Cross, A., Pearlman, A., Komissarov, I., Slysz, W., and Sobolewski, R., “Middle-infrared to visible-light ultrafast superconducting single-photon detector,” *IEEE Transactions on Applied Superconductivity* **17**(1), 246–251 (2007).
- [17] Semenov, A., Gol’tsman, G., and Korneev, A., “Quantum detection by current carrying superconducting film,” *Physica C* **352**, 349–356 (2001).
- [18] Gol’tsman, G., Okunev, O., Chulkova, G., Lipatov, A., Semenov, A., Smirnov, K., Voronov, B., Dzardanov, A., Williams, C., and Sobolewski, R., “Picosecond superconducting single-photon optical detector,” *Applied Physics Letters* **79**, 705–707 (2001).
- [19] Goltsman, G., Smirnov, K., Kouminov, P., Voronov, B., Kaurova, N., Drakinsky, V., Zhang, J., Verevkin, A., and Sobolewski, R., “Fabrication of nanostructured superconducting single-photon detectors,” *IEEE Transactions On Applied Superconductivity* **13**, 192–195 (June 2003).
- [20] Cherednichenko, S., Yagoubov, P., Il’in, K., Gol’tsman, G., and Gershenson, E., “Large bandwidth of nbn phonon cooled hot electron bolometer mixers on sapphire substrates,” *Proceedings of the 8th International Symposium on Space Terahertz Technology, Cambridge, MA, USA*, 245 (March 1997).
- [21] Milostnaya, I., Korneev, A., Rubtsova, I., Seleznev, V., Minaeva, O., Chulkova, G., Okunev, O., Voronov, B., Smirnov, K., Gol’tsman, G., Slysz, W., Wegrzecki, M., Guzewicz, M., Bar, J., Gorska, M., Pearlman, A., Kitaygorsky, J., Cross, A., and Sobolewski, R., “Superconducting single-photon detectors designed for operation at 1.55- $\mu\text{m}$  telecommunication wavelength,” *Journal of Physics: Conference Series* **43**, 1334–1337 (2006).
- [22] Rosfjord, K., Yang, J., Dauler, E., Kerman, A., Anant, V., Voronov, B., Goltsman, G., and Berggren, K., “Nanowire single-photon detector with an integrated optical cavity and anti-reflection coating,” *Optics Express* **14**(2), 527–534 (2006).
- [23] Tarkhov, M., Morozov, D., Mauskopf, P., Seleznev, V., Korneev, A., Kaurova, N., Rubtsova, I., Minaeva, O., Voronov, B., and Goltsman, G., “Single photon counting detector for thz radioastronomy,” in [*Proceedings of the 17th Inter. Symp. on Space Terahertz technol.*], (May 2006).
- [24] Korneev, A., Kouminov, P., Matvienko, V., Chulkova, G., Smirnov, K., Voronov, B., Goltsman, G., Currie, M., Lo, W., Wilsher, K., Zhang, J., Slysz, W., Pearlman, A., Verevkin, A., and Sobolewski, R., “Sensitivity and gigahertz counting performance of NbN superconducting single-photon detectors,” *Applied Physics Letters* **84**, 5338–5340 (June 2004).
- [25] Verevkin, A., Pearlman, A., Slysz, W., Zhang, J., Currie, M., Korneev, A., Chulkova, G., Okunev, O., Kouminov, P., Smirnov, K., Voronov, B., Goltsman, G., and Sobolewski, R., “Ultrafast superconducting single-photon detectors for near-infrared-wavelength quantum communications,” *Journal of Modern Optics* **51**(9-10), 1447–1458 (2004).
- [26] Kerman, A., Dauler, E., Keicher, W., Yang, J., Berggren, K., Gol’tsman, G., and Voronov, B., “Kinetic-inductance-limited reset time of superconducting nanowire photon counters,” *Applied Physisc Letters* **88**, 111116 (2006).
- [27] Slysz, W., Wegrzecki, M., Bar, J., p. Grabiec, Górska, M., Zwiller, V., Latta, C., Böhi, P., Pearlman, A., Cross, A., Pan, D., Kitaygorsky, J., Komissarov, I., Verevkin, A., Milostnaya, I., Korneev, A., Minayeva, O., Chulkova, G., Smirnov, K., Voronov, B., Goltsman, G., and Sobolewski, R., “Fibre-coupled, single photon detector based on nbn superconducting nanostructures for quantum communications,” *Journal of Modern Optics* **54**(2-3), 315–326 (2007).
- [28] Tarkhov, M., Claudon, J., Poizat, J. P., Korneev, A., Divochiy, A., Seleznev, V., Kaurova, N., Voronov, B., and Goltsman, G., “Ultrafast reset time of superconducting single photon detectors,” *Appl. Phys. Lett.* **92**, 241112 (2008). <http://link.aip.org/link/?APL/92/241112>.